Impact of Building Structure on Heat Storage Flux Estimation: An Observational Case Study in Beijing

Nana Li, Shiguang Miao, Xiaoma Li, and Junxia Dou

Abstract—The urban heat storage flux, Q_S, is one of the main drivers of the nocturnal urban heat island effect. However, the complex 3-D building structure makes observations and simulations of Q_S difficult. This study observes the 3-D surface radiant temperature (T_s) of a building in Beijing, China. The element surface temperature method (ESTM) and the half-order (HO) method are compared for Q_S simulation using T_s observations. The impact of building structure on Q_S and urban heat island intensity (UHII) are also studied. Results show the following. First, Q_S's simulated by ESTM and HO are nearly the same for walls. However, the HO method only needs one-layer exterior surface temperature, which has great potential for regional ΔQ_S simulation by satellite remote sensing data. Second, during the daytime, Q_S's of each facet are significantly different from each other. The maximum observed difference of Q_S is up to 452 W/m^2 between the roof and north wall in May 2019. Third, complete Q_S ($Q_{S,c}$) is calculated by each facet Q_S and area fraction. The relationships between UHII and both 2-D Q_S(roof Q_S) and 3-D Q_S($Q_{S,c}$) are studied. Q_S is positively correlated with nocturnal UHII, and 3-D Q_S corresponds more closely to UHII with a larger Spearman's coefficient ($p < 0.05$). This study presents the effect of building structure on heat flux and could provide an insight for future Q_S and urban heat island (UHI) studies.

Index Terms—Building 3-D structure, building heat storage, building surface temperature observation, urban heat island (UHI).

I. INTRODUCTION

THE urban heat storage flux (Q_S) is the net heat stored in the entire fabric of an urban system, including the buildings, trees, air, and ground. It is an important component of the urban surface energy balance (USEB) [1]. Q_S contributes a relatively larger fraction of the net radiation (R_n) and is approximately two to six times larger than that in nonurban canopies [2], [3]. In addition, Q_S is also a major contributor to the nocturnal urban heat island (UHI) effect [4]. R_n and turbulent fluxes could be measured by radiometry and eddy-covariance system instruments [5]–[7]. However, Q_S in an urban system is difficult to measure due to the diverse surface types and complex structures in the urban environment.

Despite these limitations, four techniques have been developed for Q_S estimation. First, the residual of the USEB equation can be used to estimate Q_S [8]. This approach is simple but has a large error in Q_S because the errors in R_n and turbulent fluxes contribute additively to Q_S [9]–[11]. Second, the objective hysteresis model (OHM) uses a hysteresis relationship between R_n and Q_S [12]. The coefficients depend on land-cover types and were empirically provided by Grimmond *et al.* [12]. Furthermore, Sun *et al.* [13] parameterized these coefficients based on the advection-diffusion equation. However, the OHM method does not consider the impact of urban structure on Q_S. Third, the heat conduction approach is more physically based but generally needs more parameters. For example, the element surface temperature method (ESTM) [6] is an area-weighted average of each component Q_S (e.g., roof, wall, road, and vegetation), requiring both exterior and interior building surface temperatures. However, the interior surface temperature is not easy to observe regionally. Fourth, a numerical model can be used, e.g., the town energy balance (TEB) model [14] that is similar to the ESTM. The numerical model is complex and involves many physical processes, resulting in some uncertainties in the estimated Q_S.

The half-order (HO) method [15], another heat conduction-based model, has been widely used for soil heat flux estimation [16], [17] but rarely for urban systems. The HO method requires only one-layer surface temperature; it has the potential to be used for regional Q_S estimation by satellite remote sensing data. If the urban "surface" is regarded as the interface with the atmosphere, is the HO method applicable for urban Q_S estimation?

Urban surface temperature (T_s) is one of the main parameters for Q_S estimation. However, due to the 3-D urban structure and diversity of urban surface thermal properties, T_s is anisotropic with a difference of more than 10 K at different observation directions [18]–[21]. This anisotropy in T_s will result in anisotropy in the estimated Q_S. However, to the best of our knowledge, there still few studies to investigate how Q_S varies by urban thermal anisotropy, as well as the impact of Q_S anisotropy on the UHI effect. Although Lindberg *et al.* [22] simulated 3-D urban Q_S, they did not consider the impact of building structure and thermal anisotropy on Q_S substantively because they used the same T_s values for roof and walls in the daytime.

The objectives of the present study as follows.
1) Carry out an experiment of 3-D building T_s observations in Beijing, China. Since the regional urban T_s is difficult to measure, buildings make a significant fraction of the
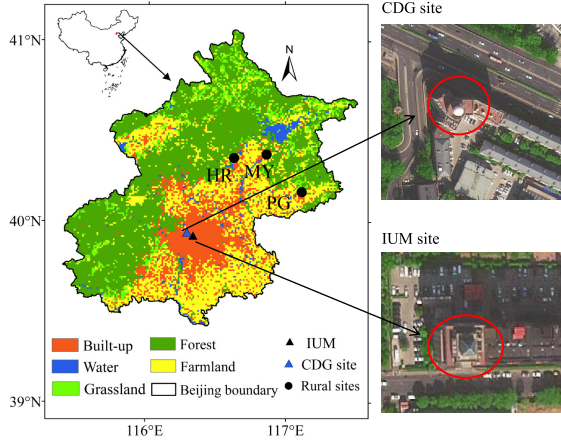
Fig. 1. Land-cover types of Beijing and locations of urban (IUM and CDG) and rural sites (HR, MY, and PG).

Fig. 2. iButton logger positions (red points) on (a) south, (b) west, (c) north facets, and (d) roof and the iButton logger.

urban surface, so a typical building is observed in this study.

2) Compare building Q_S by the ESTM and HO methods based on the observed T_s.

3) Investigate the anisotropy and diurnal variation of Q_S, e.g., roof and walls, and the impact of these variations on the UHI effect. This study will help to further understand the impact of urban structure on urban energy flux and the urban thermal environment.

II. METHODOLOGY

A. Study Area and Observations

The office building of the Institute of Urban Meteorology (IUM), China Meteorological Administration, Beijing (116.29° E, 39.94° N) (see Fig. 1), was observed in this study. The building has ten floors with thick limestone walls and a roof.

Building surface temperatures were measured with iButton temperature loggers (a DS18B20 digital thermometer, International Micronode Technology Limited, Beijing) (see Fig. 2). These devices measure temperature via temperature-dependent crystal oscillator frequencies with 0.5 °C resolution and ±0.5 °C accuracy [21]. In total, 44 iButton loggers were used in this study: 34 loggers for the exterior walls and windows; two loggers for the roof and eight loggers for the interior walls and windows. The measurements on the third, sixth, and ninth floors were averaged at each facet. The 10-min interval data were averaged over 1 h. We also used a Hyperspectral infrared camera (Hyper-Cam LW, Telops Company, Canada) for IUM T_s observation and compared it with iButton. The diurnal trend of the iButton measurements is similar to Hyper-Cam measurements. The interior building surface temperature was only observed in September 2018. Only sunny, breezy days were utilized in this study (September 11–30, 2018; May 9, 13, 16, 21, 28, and September 2–7, 2019). The air conditioning is not operating in May and September in Beijing and has no effect on UHI. This is better to investigate the relationship between heat storage and UHI.

For the UHI study, Huairou (HR), Miyun (MY), and Pinggu (PG) sites were used as rural sites [21], [23], IUM, and
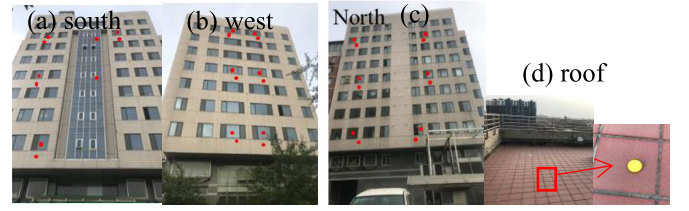
Chedaogou (CDG), 1 km away from IUM, were used as urban sites (see Fig. 1). The CDG site is on the 30-m high roof of the office building of the Beijing Meteorological Service. The morphology of IUM and CDG is similar, e.g., close to roads, and the surrounding is open, so the air temperature (T_a) of the CDG site was used as the urban temperature for UHI. The rural T_a at a 2-m height was interpolated to a 30-m horizontal grid based on the lapse rate (T_a decreases at a rate of 0.6° per 100-m increase in altitude).

B. HO Method

In this study, the building surface was regarded as the interface of the building with the atmosphere. The HO method transforms the vertical gradient of temperature to a time gradient using an HO derivative/integral operator [15].

The 1-D thermal conduction equation can be written as (1) [24]. The soil heat flux $Q(z, t)$ at depth z and time t is shown in the following equation:

$$\rho c \frac{\partial T(z,t)}{\partial t} = \lambda \frac{\partial^2 T(z,t)}{\partial z^2} \tag{1}$$

$$Q(z,t) = \lambda \frac{\partial T(z,t)}{\partial z} \tag{2}$$

where $T(z, t)$ is the temperature at depth z and time t, ρc [J/(m³K)] is the volumetric heat capacity, and λ [W/(mK)] is the thermal conductivity.

The initial and boundary conditions are shown in (3) and (4). The idealized initial condition is when the vertical temperature is constant at T_0(K). However, our previous study showed that Q_G tended to require a spin-up of one day when any time as the initial condition. Thus, the starting time is not critical. Combining (1) and (2), the heat flux at depth z and time t can be expressed as (5). A detailed derivation can be found in the literature [15]

$$T = T_0, \quad \text{for } t = 0, z \le 0 \tag{3}$$

$$T = T_0, \quad \text{for } t > 0, z \to -\infty \tag{4}$$

$$Q_S(z,t) = \sqrt{\lambda \rho c} \frac{\partial^{1/2}[T(z,t) - T_0]}{\partial t^{1/2}} = \sqrt{\frac{\lambda \rho c}{\pi}} \int_0^t \frac{dT(z,t)}{\sqrt{t-s}}. \tag{5}$$

For the building surface with $z = 0$, the heat flux is

$$Q_{S,i\_HO}(t) = \sqrt{\frac{\lambda_i \rho_i c_i}{\pi}} \int_0^t \frac{dT_i(s)}{\sqrt{t-s}} \tag{6}$$

where Q_{S,i_HO} (W/m²) is the surface heat flux of component i, T_i (K) is a component of surface temperature, s is the

integration variable, t (s) is the time, λ_i [W/(mK)] is the thermal conductivity of component i, and $(\lambda_i \rho_i c_i)^{1/2}$ is the thermal inertia that reflects the speed of the temperature change. In this study, limestone with $\lambda = 1.5$ W/(mK) and $\rho c = 2.1 \times 10^6$ J/(m^{3}K) and glass with $\lambda = 0.76$ W/(mK) and $\rho c = 2.1 \times 10^6$ J/(m^{3}K) were used. The individual components were the southern wall, the southern window, the western wall, the western window, the northern wall, the northern window, and the roof.

C. Element Surface Temperature Method

The ESTM method [6] was used to calculate $Q_{\text{S\_ESTM}}$ using

$$Q_{S,i\_\text{ESTM}}(t) = \frac{\Delta T_i'(t)}{\Delta t} \rho_i c_i \Delta z_i \qquad (7)$$

where T' (K) is the average value of the exterior and interior surface temperatures observed in this study, and Δz_i (m) is the thickness of component i. The wall (window) values of $Q_{\text{S\_ESTM}}$ at the third, sixth, and ninth floors in the same orientation were averaged to express the wall (window) $Q_{\text{S\_ESTM}}$.

Combining (1) and (2) shows that $Q_{\text{S\_ESTM}} = Q_{\text{S\_HO,exterior}} - Q_{\text{S\_HO,interior}}$. In this study, we calculated the exterior and interior surface heat fluxes, $Q_{\text{S\_HO,exterior}}$ and $Q_{\text{S\_HO,interior}}$, using the observed exterior and interior surface temperatures, respectively. The thermal parameters are not sensitive to $Q_{\text{S\_HO}}$ because λ_i and $\rho_i c_i$ were inside of the radical sign (6), reducing their impact on Q_s.

D. Complete Heat Storage Flux

The complete Q_S is expressed by (8), following the complete urban surface temperature approach proposed by Voogt et al. [25]

$$Q_{S,c} = \sum_{i=0}^{n} f_i \cdot \Delta Q_{S,i} \qquad (8)$$

where $Q_{S,c}$ (W/m^2) is the complete surface heat storage flux; $Q_{S,i}$ (W/m^2) is the ith component of the heat storage flux; f_i is the fraction of the total surface area of the building for component i; and n is the number of components ($n = 7$).

E. Urban Heat Island Intensity

The UHI intensity (UHII) is calculated by

$$\text{UHII}(t) = T_{\text{urban}}(t) - T_{\text{rural}}(t) \qquad (9)$$

where $T_{\text{urban}}(t)$ is the air temperature at a 30-m height measured at the CDG station at time t; T_{rural} (t) is the average air temperature at a 30-m height of three rural sites at time t.

III. Results and Discussion

A. Comparing Heat Storage Fluxes Calculated Using the HO and ESTM Methods

The average diurnal variation of $Q_{\text{S\_HO}}$ and $Q_{\text{S\_ESTM}}$ during 11–30 September for walls [see Fig. 3(a)] and windows [see Fig. 3(b)] are compared. For walls, $Q_{\text{S\_HO}}$ and $Q_{\text{S\_ESTM}}$ are very similar, but, for windows, $Q_{\text{S\_ESTM}}$ is much smaller than
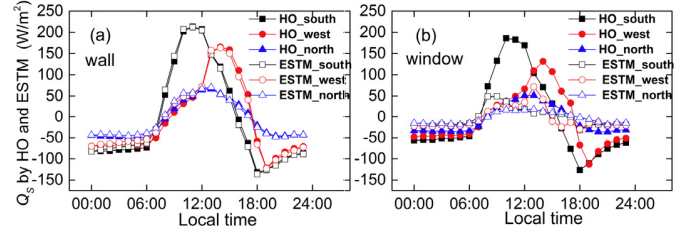
Fig. 3. Hourly average of $Q_{\text{S\_HO}}$ and $Q_{\text{S\_ESTM}}$ for (a) walls and (b) windows during 11–30 September, 2018.
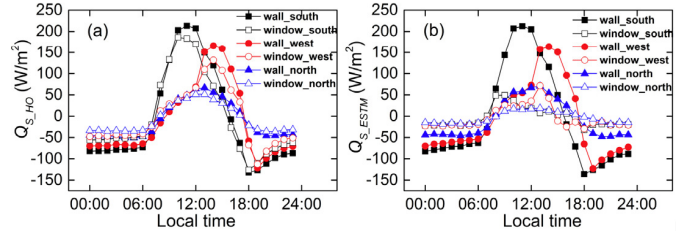

Fig. 4. Hourly average of $Q_{\text{S\_HO}}$ and $Q_{\text{S\_ESTM}}$ during 11–30 September, 2018.

$Q_{\text{S\_HO}}$(see Fig. 3). The maximum difference between $Q_{\text{S\_HO}}$ and $Q_{\text{S\_ESTM}}$ is 165 W/m^2 for windows on the south side at 11:00 A.M., while it is 22 W/m^2 for the wall on the west side at 9:00 A.M. This indicates that the solar heat was primarily intercepted by walls, with only a little heat entering the room through the wall. The windows are thin and transparent; most heat penetrates the glass, and only a little is stored. In addition, the hysteresis in $Q_{\text{S\_HO}}$ and $Q_{\text{S\_ESTM}}$ on different facets is caused directly by the characteristics of the building surface temperatures. The detailed information of T_s anisotropy is described in our earlier study [21].

The difference in $Q_{\text{S\_HO}}$ between walls and windows varies with orientation. For example, the maximum difference is 48 W/m^2 on the south side, 51 W/m^2 on the west side, and 17 W/m^2 on the north side [see Fig. 4(a)]. However, this difference in $Q_{\text{S\_ESTM}}$ is much larger than that calculated from $Q_{\text{S\_HO}}$. For example, the difference in $Q_{\text{S\_ESTM}}$ between walls and windows was a maximum of 194 W/m^2 on the south side, 162 W/m^2 on the west side, and 52 W/m^2 on the north side [see Fig. 4(b)]. Therefore, $Q_{\text{S\_ESTM}}$ is more sensitive to building materials than $Q_{\text{S\_HO}}$. When urban heat storage is estimated by the ESTM method, the classification of wall and window should be distinguished rigorously.

B. Impact of Building Structure on Q_S

Significantly, building $Q_{\text{S\_HO}}$ and $Q_{\text{S\_ESTM}}$ are both anisotropic because building surfaces at different orientations receive different solar radiation intensities and durations. $Q_{\text{S\_HO}}$ and $Q_{\text{S\_ESTM}}$ are nearly the same for solid surfaces (e.g., walls), and the anisotropic characteristics are similar. Moreover, $Q_{\text{S\_HO}}$ is estimated more easily than $Q_{\text{S\_ESTM}}$ because the ESTM method does not need the interior surface T_s, which is difficult to obtain for all of the buildings in a regional urban system. Only $Q_{\text{S\_HO}}$ is analyzed in this section. Data for 2019 are used here because roof measurements were not recorded in 2018.
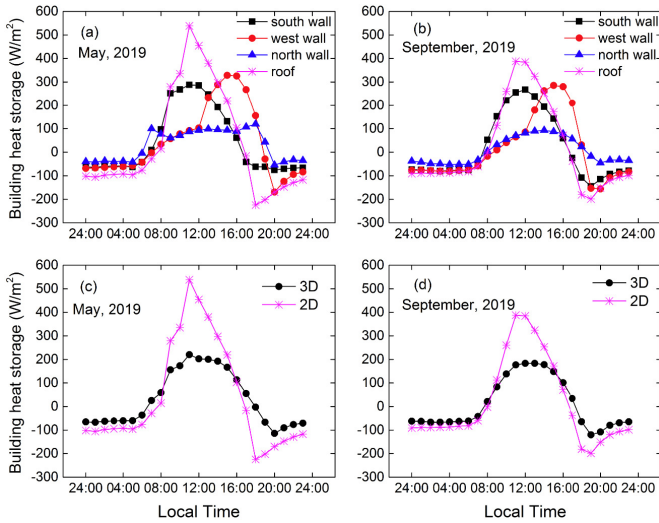
Fig. 5. Hourly average of each component Q_S by the HO method during (a) May 9, 13, 16, 21, 28, 2019, and (b) September 2–7, 2019. (c) and (d) Comparison of 2-D (roof) and 3-D Q_S ($Q_{S,c}$).

The roof has the largest Q_S during daytime and nighttime. This shows that the roof absorbs more energy during the day and releases more energy at night [see Fig. 5(a) and (b)] compared with other surfaces of the building. The difference in Q_S between each facet during the day is larger than that at night [see Fig. 5(a) and (b)] because the Q_S anisotropy is mainly caused by solar anisotropy. The maximum difference of Q_S appears between the roof and the north wall with a difference of 452 W/m^2 in May and 318 W/m^2 in September. The building structure affected not only Q_S but also the time when the maximum Q_S occurs. For example, the roof Q_S reaches a maximum value at 11:00, but the north wall maximum occurs at 15:00 [see Fig. 5(b)].

The complete surface heat flux $Q_{S,c}$ is calculated based on (8), using each component Q_S and the area fraction of each component. The roof Q_S is regarded as "2-D" and $Q_{S,c}$ as "3-D." The 3-D Q_S is much smaller than the 2-D Q_S during the daytime. The maximum difference between 2-D and 3-D Q_S can be up to 318 W/m^2 in May and 211 W/m^2 in September [see Fig. 5(c) and (d)]. Thus, there will be large errors associated with regional 2-D estimations of Q_S calculated from satellite remote sensed surface temperature alone.

C. Relationship Between Q_S and UHII

Q_S's of rural sites are calculated by the HO method, using *in situ* observations of land surface temperature, soil water content, and soil porosity. The detailed information is presented in the Supplementary Material. The difference of Q_S between IUM sites and rural sites is compared with UHII (see Table I). During the nighttime, 3-D Q_S is significantly related to UHII with $p < 0.05$ and more correlated with UHII than 2-D Q_S with a larger Spearman's coefficient. This shows that the building structure would affect nocturnal UHI. During the daytime, 2-D and 3-D Q_S's are both significantly related to UHII with negative coefficients. This shows that lower Q_S may reduce nocturnal UHI, and higher Q_S may reduce daytime

TABLE I
SPEARMAN'S CORRELATION COEFFICIENTS BETWEEN UHII AND Q_S IN MAY 9, 13, 16, 21, 28, 2019

	UHII VS. 2-D Q_S	UHII VS. 3-D Q_S
DAY	-0.38*	-0.41*
NIGHT	0.26	0.42*
WHOLE DAY	0.12	0.29*

*: correlation is significant at the 0.05 level.

UHI. Modest Q_S's could reduce diurnal UHI and lead to the cooling effect.

D. Limitation and Future Work

Some uncertainties and limitations remain in this study. First, only one building was used in the present study, so it was not possible to reveal the impact of urban form (building density, sky view factor, and so on) on building thermal anisotropy and heat storage flux. Further experiments should be carried out in a regional urban area with more buildings in different local climate zones (LCZs) and across more urban cover types, e.g., road, water, and vegetation. Then, 3-D Q_S and UHII could be studied at a city scale. Second, the iButton logger is a contact sensor and has general problems associated with this type of sensor. For example, the sensor covers the measured area and will block part of the solar radiation, which may affect the observed values. However, this study mainly focuses on the building thermal anisotropy–thermal characteristics of building faces with different orientations. Hence, absolute observation values would have little impact on the results. In the future, noncontact sensors (e.g., SI-111 thermal infrared temperature sensors or thermal infrared cameras) would be recommended to calibrate the iButtons or observe the surface temperatures instead of iButtons. Third, the eastern facet T_s was not measured in this study because it was joined to another building, potentially leading to an underestimation of the complete heat storage values. However, the roof T_s dominates Q_c values, so the missing eastern facet T_s may only affect Q_c weakly. Nevertheless, all the building facets should be measured simultaneously in further studies.

IV. CONCLUSION

The complex urban structure has an important impact on the urban thermal environment. It is difficult to observe urban 3-D surface temperature T_s. This study observed a building 3-D T_s using iButton loggers and investigated how the building structure affects building heat storage flux Q_S. In addition, ESTM and HO methods for Q_S estimation were compared using T_s observations. The relationship between Q_S and UHII was also explored. According to the author's previous study [21], the T_s difference between different facets at the same time, and it can be up to 18 K. This thermal anisotropy will affect Q_S calculation.

For walls, Q_S's calculated by the two methods are nearly the same, but, for windows, Q_S has a large difference. The walls are thick enough to intercept most of the solar heat into the room, and consequently, most of the incident heat is stored in

the wall. However, windows are thin and transparent, so most of the energy incident of the windows is transmitted into the room. The energy transmitted into the room is represented in Q_S estimated by the HO method but not that estimated by the ESTM. Moreover, the HO method only requires exterior surface temperature, but ESTM requires both exterior and interior surface temperature. When the 3-D urban surface is regarded as the interface with the atmosphere, the HO method is potential for regional urban Q_S estimation using land surface temperature by satellite remote sensing technology.

The daytime Q_S for each facet of the building has large differences with a maximum of 452 W/m^2 between roof and north wall in May and 318 W/m^2 in September 2019. Q_S of each building facet is different largely during the daytime. This is caused by building thermal anisotropy, which affects not only Q_S values but also the time that the maximum Q_S occurred. The maximum Q_S occurs earliest for the roof, followed by the south wall, then the west wall, and, finally, the north wall. The complete heat storage flux $Q_{S,c}$(3-D Q_S) was compared with the roof Q_S (2-D Q_S). The 3-D Q_S is smaller than 2-D Q_S with a maximum difference of 318 W/m^2 during daytime in May 2019. The building absorbs heat during the daytime and releases heat at night, which enhances nocturnal UHII. Q_S is positively related to UHII during nighttime and negatively during the daytime. 3-D Q_S is more closely correlated with UHII than 2-D Q_S, with a larger Spearman's coefficient. Although only one building Q_S was studied, this study provides an insight into future heat fluxes and UHI estimations.

The urban thermal anisotropy caused by surface 3-D structure and geometric relationship between the sun and urban surface and affects surface heat storage flux and UHII significantly. There will be some significant errors if only 2-D surface thermal characteristics (i.e., land surface temperature from the satellite remote sensing data) are used for urban heat flux and UHI studies. The urban thermal anisotropy should be taken into account for urban thermal environment studies. The satellite measurement of the 3-D urban surface temperature is a key issue to be addressed, which is important and essential for refined thermal environment studies at a city scale. In addition, the nocturnal UHI is expected to be decreased using some materials with low thermal inertia, leading to low Q_S.

ACKNOWLEDGMENT

REFERENCES

[1] T. R. Oke, G. Mills, A. Christen, and J. Voogt, *Urban Climates*. Cambridge, U.K.: Cambridge Univ. Press, 2017.

[2] T. R. Oke, *Boundary Layer Climates*. New York, NY, USA: Routledge, 1987.

[3] C. S. B. Grimmond and T. R. Oke, "Heat storage in urban areas: Local-scale observations and evaluation of a simple model," *J. Appl. Meteorol.*, vol. 38, pp. 922–940, Jul. 1999, doi: 10.1175/1520-0450(1999)038<0922:HSIUAL>2.0.CO;2.

[4] T. R. Oke, G. T. Johnson, D. G. Steyn, and I. D. Watson, "Simulation of surface urban heat islands under 'ideal' conditions at night part 2: Diagnosis of causation," *Boundary-Layer Meteorol.*, vol. 56, no. 4, pp. 339–358, Sep. 1991, doi: 10.1007/bf00119211.

[5] V. R. N. Pauwels and E. Daly, "Advantages of analytically computing the ground heat flux in land surface models," *Hydrol. Earth Syst. Sci.*, vol. 20, no. 11, pp. 4689–4706, Nov. 2016, doi: 10.5194/hess-20-4689-2016.

[6] B. Offerle, C. S. B. Grimmond, and K. Fortuniak, "Heat storage and anthropogenic heat flux in relation to the energy balance of a central European city centre," *Int. J. Climatol.*, vol. 25, no. 10, pp. 1405–1419, Aug. 2005.

[7] S. M. Roberts, T. R. Oke, C. S. B. Grimmond, and J. A. Voogt, "Comparison of four methods to estimate urban heat storage," *J. Appl. Meteorol. Climatol.*, vol. 45, no. 12, pp. 1766–1781, Dec. 2006, doi: 10.1175/JAM2432.1.

[8] S. Kato and Y. Yamaguchi, "Estimation of storage heat flux in an urban area using ASTER data," *Remote Sens. Environ.*, vol. 110, no. 1, pp. 1–17, Sep. 2007, doi: 10.1016/j.rse.2007.02.011.

[9] X. Ao *et al.*, "Heat, water and carbon exchanges in the tall megacity of Shanghai: Challenges and results," *Int. J. Climatol.*, vol. 36, no. 14, pp. 4608–4624, Nov. 2016, doi: 10.1002/joc.4657.

[10] D. Li, T. Sun, M. Liu, L. Yang, L. Wang, and Z. Gao, "Contrasting responses of urban and rural surface energy budgets to heat waves explain synergies between urban heat islands and heat waves," *Environ. Res. Lett.*, vol. 10, no. 5, May 2015, Art. no. 054009.

[11] T. R. Oke and H. A. Cleugh, "Urban heat storage derived as energy balance residuals," *Boundary-Layer Meteorol.*, vol. 39, no. 3, pp. 233–245, May 1987, doi: 10.1007/bf00116120.

[12] C. S. B. Grimmond, H. A. Cleugh, and T. R. Oke, "An objective urban heat storage model and its comparison with other schemes," *Atmos. Environ. B, Urban Atmos.*, vol. 25, no. 3, pp. 311–326, Jan. 1991.

[13] T. Sun, Z.-H. Wang, W. C. Oechel, and S. Grimmond, "The analytical objective hysteresis model (AnOHM v1.0): Methodology to determine bulk storage heat flux coefficients," *Geosci. Model Develop.*, vol. 10, no. 7, pp. 2875–2890, Jul. 2017, doi: 10.5194/gmd-10-2875-2017.

[14] V. Masson, "A physically-based scheme for the urban energy budget in atmospheric models," *Boundary-Layer Meteorol.*, vol. 94, no. 3, pp. 357–397, Mar. 2000.

[15] J. Wang and R. L. Bras, "Ground heat flux estimated from surface soil temperature," *J. Hydrol.*, vol. 216, pp. 214–226, Mar. 1999, doi: 10.1016/S0022-1694(99)00008-6.

[16] H. Hu, N. Li, F. Tian, and Q. Tie, "Modification of harmonic analysis model for diurnal surface soil heat flux estimate from multiple remote sensing data," *J. Appl. Remote Sens.*, vol. 12, 2018, Art. no. 036009.

[17] C.-I. Hsieh, C.-W. Huang, and G. Kiely, "Long-term estimation of soil heat flux by single layer soil temperature," *Int. J. Biometeorol.*, vol. 53, no. 1, pp. 113–123, Jan. 2009, doi: 10.1007/s00484-008-0198-8.

[18] J. P. Lagouarde *et al.*, "Modelling daytime thermal infrared directional anisotropy over Toulouse city centre," *Remote Sens. Environ.*, vol. 114, pp. 87–105, Jan. 2010, doi: 10.1016/j.rse.2009.08.012.

[19] W. Zhan *et al.*, "Assessment of thermal anisotropy on remote estimation of urban thermal inertia," *Remote Sens. Environ.*, vol. 123, pp. 12–24, Aug. 2012, doi: 10.1016/j.rse.2012.03.001.

[20] J. A. Voogt, "Assessment of an urban sensor view model for thermal anisotropy," *Remote Sens. Environ.*, vol. 112, pp. 482–495, Feb. 2008, doi: 10.1016/j.rse.2007.05.013.

[21] N. Li and X. Li, "The impact of building thermal anisotropy on surface urban heat island intensity estimation: An observational case study in Beijing," *IEEE Geosci. Remote Sens. Lett.*, vol. 17, no. 12, pp. 2030–2034, Dec. 2020, doi: 10.1109/LGRS.2019.2962383.

[22] F. Lindberg, K. F. G. Olofson, T. Sun, C. S. B. Grimmond, and C. Feigenwinter, "Urban storage heat flux variability explored using satellite, meteorological and geodata," *Theor. Appl. Climatol.*, vol. 141, nos. 1–2, pp. 271–284, Jul. 2020, doi: 10.1007/s00704-020-03189-1.

[23] J. Wang, Z. Yan, Z. Li, W. Liu, and Y. Wang, "Impact of urbanization on changes in temperature extremes in Beijing during 1978–2008," *Chin. Sci. Bull.*, vol. 58, no. 36, pp. 4679–4686, Dec. 2013, doi: 10.1007/s11434-013-5976-y.

[24] H. S. Carslaw and J. C. Jaeger, *Conduction of Heat in Solids*. Oxford, U.K.: Clarendon, 1959, pp. 64–70.

[25] J. A. Voogt and T. R. Oke, "Complete urban surface temperatures," *J. Appl. Meteorol.*, vol. 36, pp. 1117–1132, Sep. 1997, doi: 10.1175/1520-0450(1997)036<1117:cust>2.0.co;2.